

Analysis and Compensation of Carrier Frequency Offset Impairments in Unique Word OFDM

Christian Hofbauer, *Member, IEEE*, Werner Haselmayr, *Member, IEEE*, Hans-Peter Bernhard, *Senior Member, IEEE*, and Mario Huemer, *Senior Member, IEEE*

Abstract—Unique Word-orthogonal frequency division multiplexing (UW-OFDM) is known to provide various performance benefits over conventional cyclic prefix (CP) based OFDM. Most important, UW-OFDM features excellent spectral sidelobe suppression properties and an outstanding bit error ratio (BER) performance. Carrier frequency offset (CFO) induced impairments denote a challenging task for OFDM systems of any kind. In this work we thoroughly investigate the CFO effects on UW-OFDM and compare it to conventional OFDM. Different CFO compensation approaches with different computational complexity are considered throughout this work, assessed against each other, and the residual CFO error of these approaches is analyzed by deriving analytical error models. A mean squared error analysis carried out after data estimation reveals a significantly higher robustness of UW-OFDM over CP-OFDM against CFO effects. Additionally, the conducted BER simulations generally support this conclusion for various scenarios, ranging from uncoded to coded transmission in a frequency selective environment.

Index Terms—UW-OFDM, CP-OFDM, unique word, pilot tone, carrier frequency offset

I. INTRODUCTION

In Unique Word (UW)-OFDM, introduced in [1], the conventional cyclic prefix (CP) in the guard interval is replaced by a deterministic sequence – the UW. The introduction of the UW within the interval of the discrete Fourier transform (DFT) entails the introduction of redundancy in the frequency domain, which can beneficially be utilized to obtain superior spectral shaping characteristics [2], [3], [4], [5] or outstanding bit error ratio (BER) performance for linear [6], [2], [7], [8], [9], non-linear [10], [11], [12], [13], iterative¹ [16], [17] as well as neural network (NN) [18], [19] based receivers.

Various other approaches known as PRP-OFDM (pseudo-random prefix) [20], KSP-OFDM (known symbol padding) [21], OFDM with a PN (pseudo noise) sequence [22], TDS-OFDM (time domain synchronous) [23], [24], [22], or even OFDM with Unique Word [25] implement deterministic sequences in the guard interval. Sharing with UW-OFDM the common idea of a deterministic sequence in the guard interval,

The authors are with the Silicon Austria Labs GmbH, Linz, Austria (christian.hofbauer@silicon-austria.com, hans-peter.bernhard@silicon-austria.com), with the Institute of Signal Processing, Johannes Kepler University Linz, Linz, Austria (mario.huemer@jku.at), and with the Institute for Communications Engineering and RF-Systems, Johannes Kepler University Linz, Linz, Austria (werner.haselmayr@jku.at), respectively.

This work has been supported by Silicon Austria Labs (SAL), owned by the Republic of Austria, the Styrian Business Promotion Agency (SFG), the federal state of Carinthia, the Upper Austrian Research (UAR), and the Austrian Association for the Electric and Electronics Industry (FEEL).

¹The term *iterative receiver* refers to an iterative exchange of reliability information between detector and decoder [14], [15].

only UW-OFDM implements it inside the DFT, and thus solely benefits from the introduced redundancy and the resulting beneficial properties.

So far, investigations of UW-OFDM have primarily focused on principle performance bounds and were based on various idealized assumptions, such as perfect timing, carrier phase or carrier frequency synchronization. Investigations aside from idealized scenarios have been limited to the impact of imperfect channel estimation on the BER behavior [2], peak to average power ratio (PAPR) and peak to minimum power ratio (PMR) analyses [26], [27], [28], as well as feasibility considerations in terms of computational complexity [6], [29].

A major challenge in OFDM arises from a carrier frequency offset (CFO), which makes accurate estimation and compensation of this offset essential. This task is often divided into an acquisition phase providing an initial rough correction of the entire packet based on the preamble [30], and a subsequent tracking phase for a finer correction on a symbol-by-symbol basis. In this paper, we only address the tracking phase.

Existing work on UW based systems together with CFO considerations focused on the time domain based estimation thereof based on UWs [31], [32], [33], [34], [35], mainly in context of UW based single-carrier systems. In [36], [37] we extended considerations to UW based OFDM systems with frequency pilot tone assisted CFO estimation.

In this work, all CFO related estimation tasks rely on pilot frequency tones as presented in [36], [37] rather than on UWs. Therefore, the same estimation method can be applied to all considered systems, i.e., also to non-UW based reference systems, thus ensuring a fair comparison among them. As such, an investigation of UWs for estimation purposes is not within the scope of this work. UWs in this work are limited to evaluations on how they might degrade the system performance as a result of their erroneous handling in the receiver due to CFO. For all investigations in this work, we assume a CFO to stay constant during transmission as well as a perfect timing synchronization enabling perfect packet detection.

In this work, we aim at analyzing the impact of a CFO on the performance of UW-OFDM based systems, whereas the main contributions can be summarized as follows². We elaborate on various CFO compensation approaches and assess their performance w.r.t. computational complexity and CFO compensation capabilities. We derive analytical mod-

²We note that this work is based on unpublished parts of the PhD thesis in [38].

els describing the residual error after CFO compensation, which can further be utilized as a reliability information in a communication system. Finally, we conduct BER simulations of a whole communication chain in different variants (with different combinations of coding rate and modulation alphabet) in order to assess the performance also on a system level. Throughout all evaluations, classical CP-OFDM serves as a reference.

We note that this work expands its conference version [39] in various aspects. While the main focus in [39] was laid on the analysis of the different CFO effects on various UW-OFDM setups, this work rather focuses on handling those in the context of a whole UW-OFDM based transceiver system. Besides conventional common phase error (CPE) correction already addressed in [39], we additionally consider more sophisticated CFO compensation methods that take into account all CFO induced impairments. We develop computational complexity reduced variants of thereof and compare their performance against the original implementation. Moreover, we extend performance assessment from mean squared error (MSE) considerations in [39] to evaluations at system level by means of BER simulations. For this, we additionally develop accurate analytical error models for the different CFO compensation methods and utilize them to provide reliability information to the channel decoder at the receiver.

The remainder of this work is organized as follows. We start with a recap of the UW-OFDM signaling model incorporating a CFO in Sec. II. In Sec. III, we investigate the remaining impact of these effects on the UW-OFDM performance by means of MSE analyses after applying different CFO compensation approaches. Subsequently, in Sec. IV we derive analytical models for the residual CFO error remaining from the different approaches presented in Sec. III. Next, we evaluate the CFO impact on the overall system performance in terms of BER simulations in Sec. V, and we finally conclude our work in Sec. VI.

Notation: We use lower case and upper case letters in bold face (\mathbf{a} , \mathbf{A}) to express vectors and matrices, respectively. A tilde ($\tilde{\mathbf{a}}$, $\tilde{\mathbf{A}}$) shall indicate frequency domain variables. We address with $a[k]$ element k of a vector \mathbf{a} , $[\mathbf{A}]_{k,l}$ refers to the element of the k th row and l th column, $[\mathbf{A}]_{k,*}$ corresponds to all elements of row k , and $[\mathbf{A}]_{*,l}$ all elements of column l . We use $(\cdot)^T$ for the transpose, $(\cdot)^H$ for the conjugate transpose or Hermitian, $\mathbb{E}\{\cdot\}$ for expectation, $\text{diag}(\mathbf{A})$ for the main diagonal elements of \mathbf{A} , $\text{tr}(\mathbf{A})$ to express the trace operator, and $(\cdot)^\dagger$ to denote a Moore-Penrose Pseudo-Inverse. Identity and zero matrices are denoted as \mathbf{I} and $\mathbf{0}$, respectively. A vector $\mathbf{a} \sim \mathcal{CN}(\boldsymbol{\mu}, \mathbf{C})$ denotes a circularly symmetric complex Gaussian noise vector with mean $\boldsymbol{\mu}$ and covariance matrix \mathbf{C} . We denote an estimation of \mathbf{a} as $\hat{\mathbf{a}}$. We indicate the motivation behind a specific subscript/superscript of \mathbf{a}_m by underlining a letter accordingly. Representation in equivalent complex baseband applies to all signals and systems.

II. UW-OFDM SIGNALING MODEL

In this section, we briefly review the UW-OFDM signaling model. For details, the interested reader is referred to [36].

Let $\mathbf{x}_u \in \mathbb{C}^{N_u \times 1}$ denote the UW, which we use to fill the guard interval of length $N_g = N_u$ and that is part of each OFDM time domain symbol of size N (see Fig. 1). We therefore introduce $\mathbf{x}' = [\mathbf{x}_{pl}^T \ \mathbf{x}_u^T]^T$, $\mathbf{x}' \in \mathbb{C}^{N \times 1}$,

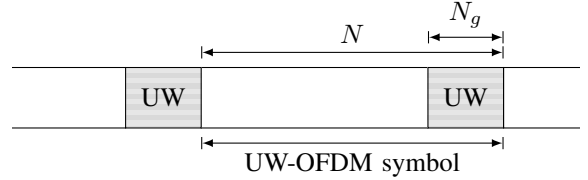


Figure 1: Structure of an UW-OFDM time domain symbol.

whereas $\mathbf{x}_{pl} \in \mathbb{C}^{(N-N_u) \times 1}$ carries the payload. Following transmission energy arguments in [40], we obtain \mathbf{x}' by generating $\mathbf{x} = [\mathbf{x}_{pl}^T \ \mathbf{0}^T]^T$ first and then add the UW with $\mathbf{x}' = \mathbf{x} + [\mathbf{0}^T \ \mathbf{x}_u^T]^T$. As in conventional OFDM, unused N_z zero subcarriers for spectral shaping reasons, N_p pilot symbols $\mathbf{p} \in \mathbb{C}^{N_p \times 1}$ for estimation purposes, and N_d data symbols $\mathbf{d} \in \mathcal{A}^{N_d \times 1}$ drawn from an alphabet \mathcal{A} form an OFDM frequency domain symbol $\tilde{\mathbf{x}} \in \mathbb{C}^{N \times 1}$. In order to account for the zero-word of the UW-OFDM time domain symbol \mathbf{x} and thus fulfill the system of equations $\mathbf{F}_N^{-1} \tilde{\mathbf{x}} = [\mathbf{x}_{pl}^T \ \mathbf{0}^T]^T$, whereas \mathbf{F}_N^{-1} is an N -point inverse DFT with $\mathbf{F}_N^{-1} = \frac{1}{N} \mathbf{F}_N^H$ and $[\mathbf{F}_N]_{k,l} = e^{-j \frac{2\pi}{N} kl}$, we have to reduce N_d by at least N_u , and instead introduce some form of redundancy. We therefore define a data generator matrix $\mathbf{G}_d \in \mathbb{C}^{(N_d+N_r+N_p) \times N_d}$ and a pilot generator matrix $\mathbf{G}_p \in \mathbb{C}^{(N_d+N_r+N_p) \times N_p}$ with $N_r = N_u$ and $N = N_d + N_r + N_p + N_z$, yielding

$$\mathbf{x} = \mathbf{F}_N^{-1} (\mathbf{B} \mathbf{G}_d \mathbf{d} + \mathbf{B} \mathbf{G}_p \mathbf{p}) = \begin{bmatrix} \mathbf{x}_{pl} \\ \mathbf{0} \end{bmatrix}, \quad (1)$$

while $\mathbf{B} \in \{0, 1\}^{N \times (N-N_z)}$ accounts for the zero subcarrier insertion.

Matrix \mathbf{G}_d in (1) maps the data symbols \mathbf{d} on the UW-OFDM symbol, while at the same time accounting for the fulfillment of the zero-word constraint. There are several degrees of freedom in designing \mathbf{G}_d , yielding realizations with different properties (see details in [2], [36]). We thus show two exemplary realizations of \mathbf{G}_d in Fig. 2 to indicate the comprehensive set of generator matrices, and we will use them as a basis for discussions in the subsequent sections. Matrix \mathbf{G}'_d in Fig. 2a has (energy relevant) entries primarily on the main diagonal. Consequently, a single data symbol is mainly mapped onto a single subcarrier, however, some parts are also spread on neighboring subcarriers, which in turn will generate the zero-word. The design and also resulting behavior of \mathbf{G}'_d is similar to a conventional OFDM system, which would in the given signal framework represented by a matrix solely with main diagonal entries. In contrast, \mathbf{G}''_d shown in Fig. 2b spreads each data symbol almost uniformly over all subcarriers and thus behaves similar to a single-carrier (SC) based system.

Matrix \mathbf{G}_p in (1) maps the pilot symbols \mathbf{p} on the UW-OFDM symbol, again accounting for the generation of the zero-word (see [36] for details on the design). Fig. 3 shows the resulting \mathbf{G}_p for the setup given in Tab. I in Sec. V-A.

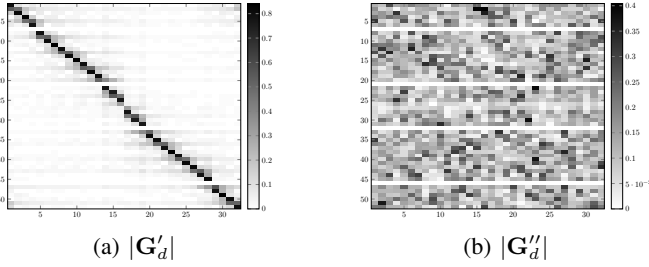


Figure 2: Exemplary data generator matrices \mathbf{G}'_d and \mathbf{G}''_d .

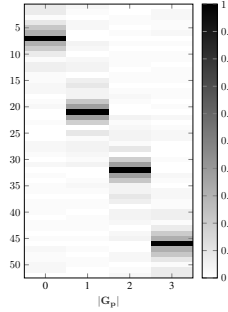


Figure 3: Exemplary pilot generator matrix \mathbf{G}_p .

With (1), the l th frequency domain UW-OFDM transmit signal follows as

$$\tilde{\mathbf{x}}^{(l)} = \mathbf{F}_N \mathbf{x}'^{(l)} = \mathbf{B} \mathbf{G}_d \mathbf{d}^{(l)} + \mathbf{B} \mathbf{G}_p \mathbf{p} + \tilde{\mathbf{x}}_u, \quad (2)$$

whereas $\tilde{\mathbf{x}}_u = \mathbf{F}_N [\mathbf{0}^T \quad \mathbf{x}_u^T]^T$ denotes the UW in the frequency domain.

The OFDM frequency domain symbol at the receiver $\tilde{\mathbf{y}}_r^{(l)}$ can be modelled as³

$$\tilde{\mathbf{y}}_r^{(l)} = \tilde{\mathbf{\Lambda}}'^{(l)} \tilde{\mathbf{H}}' \tilde{\mathbf{x}}^{(l)} + \mathbf{v}', \quad (3)$$

with $\tilde{\mathbf{H}}' \in \mathbb{C}^{N \times N}$ corresponding to the diagonal channel frequency response matrix, $\mathbf{v}' \sim \mathcal{CN}(\mathbf{0}, \sigma_v^2 \mathbf{I})$, $\mathbf{v}' \in \mathbb{C}^{N \times 1}$, and the frequency domain representation of the CFO effects given as [36]

$$\tilde{\mathbf{\Lambda}}'^{(l)} = e^{j\varphi_l} \tilde{\mathbf{\Lambda}}'_{\text{stat}}, \quad \tilde{\mathbf{\Lambda}}'^{(l)} \in \mathbb{C}^{N \times N} \quad (4)$$

and

$$\varphi_l = \frac{2\pi\epsilon}{N} \left(Nl + \frac{N-1}{2} + N_x \right), \quad (5)$$

$$\left[\tilde{\mathbf{\Lambda}}'_{\text{stat}} \right]_{k,m} = \frac{\sin(\pi(m+\epsilon-k))}{N \sin\left(\frac{\pi(m+\epsilon-k)}{N}\right)} e^{j\frac{\pi(m-k)(N-1)}{N}}. \quad (6)$$

Here, $\epsilon = \frac{f_{\text{CFO}}}{\Delta_f}$ denotes a CFO f_{CFO} normalized to the subcarrier spacing Δ_f , and φ_l carries the phase offset accumulated by previous OFDM symbols up to and including symbol l and an arbitrary offset $N_x \in \mathbb{Z}$. In summary, a frequency domain symbol suffers from a phase offset φ_l also referred to as CPE, an attenuation determined by the entries on the main diagonal

³In this work, the notation $'$ serves either as a naming convention for different generator matrix instances or to differentiate between matrices incorporating all or only the subset of non-zero subcarriers (e.g., $\tilde{\mathbf{H}}'$ versus $\tilde{\mathbf{H}}$).

of $\tilde{\mathbf{\Lambda}}'_{\text{stat}} \in \mathbb{C}^{N \times N}$, and a deviation as a result of intercarrier interference (ICI) represented by the off-diagonal entries of $\tilde{\mathbf{\Lambda}}'_{\text{stat}}$. The notation static stems from the independence of l .

III. CFO ESTIMATION AND COMPENSATION IN UW-OFDM

In the following, we will evaluate the impact of CFO effects on the UW-OFDM performance. For that we will apply different CFO compensation methods and evaluate the performance by conducting an MSE analysis after data estimation. Please note that CFO compensation by means of CPE correction presented in Sec. III-A has already been part in the conference version of this work [39]. However, we included it in a compressed form as a frame of reference for the advanced compensation methods in Sec. III-B, as well as for the derivations of the error model in Sec. IV.

We start with a removal of the zero subcarriers and extract the payload carrying subcarriers, which can be well approximated⁴ by [36]

$$\begin{aligned} \tilde{\mathbf{y}}_{pl}^{(l)} &= \mathbf{B}^T \tilde{\mathbf{y}}_r^{(l)} \\ &\approx \tilde{\mathbf{\Lambda}}^{(l)} \tilde{\mathbf{H}} \mathbf{G}_d \mathbf{d}^{(l)} + \tilde{\mathbf{\Lambda}}^{(l)} \tilde{\mathbf{H}} \mathbf{G}_p \mathbf{p} + \tilde{\mathbf{\Lambda}}^{(l)} \tilde{\mathbf{H}} \mathbf{B}^T \tilde{\mathbf{x}}_u + \mathbf{v}, \end{aligned} \quad (7)$$

where $\mathbf{v} = \mathbf{B}^T \mathbf{v}' \sim \mathcal{CN}(\mathbf{0}, \sigma_v^2 \mathbf{I})$, $\mathbf{v} \in \mathbb{C}^{(N-N_z) \times 1}$, $\tilde{\mathbf{H}} = \mathbf{B}^T \tilde{\mathbf{H}}' \mathbf{B}$, $\tilde{\mathbf{H}} \in \mathbb{C}^{(N-N_z) \times (N-N_z)}$, $\tilde{\mathbf{\Lambda}}^{(l)} = \mathbf{B}^T \tilde{\mathbf{\Lambda}}'^{(l)} \mathbf{B}$, and $\tilde{\mathbf{\Lambda}}^{(l)} \in \mathbb{C}^{(N-N_z) \times (N-N_z)}$. We note that $\tilde{\mathbf{H}}$ and $\tilde{\mathbf{\Lambda}}^{(l)}$ coincide with $\tilde{\mathbf{H}}'$ and $\tilde{\mathbf{\Lambda}}'^{(l)}$, respectively, except for excluded rows and columns at the positions of zero subcarriers. In the following, this signaling model serves as a starting point for the evaluation of different CFO compensation methods.

A. CPE correction

A common means to combat CFO impairments is CPE correction by derotating with an estimate $\hat{\varphi}_l$. Together with the subtraction of the offset

$$\mathbf{x}_{\text{off}} = \tilde{\mathbf{H}} \mathbf{G}_p \mathbf{p} + \tilde{\mathbf{H}} \mathbf{B}^T \tilde{\mathbf{x}}_u \quad (8)$$

from (7) we yield

$$\begin{aligned} \tilde{\mathbf{y}}^{(l)} &= e^{-j\hat{\varphi}_l} \tilde{\mathbf{y}}_{pl}^{(l)} - \mathbf{x}_{\text{off}} \\ &= e^{-j\hat{\varphi}_l} \tilde{\mathbf{\Lambda}}^{(l)} \tilde{\mathbf{H}} \mathbf{G}_d \mathbf{d}^{(l)} + \left(e^{-j\hat{\varphi}_l} \tilde{\mathbf{\Lambda}}^{(l)} - \mathbf{I} \right) \tilde{\mathbf{H}} \mathbf{G}_p \mathbf{p} \end{aligned} \quad (9)$$

$$\begin{aligned} &+ \left(e^{-j\hat{\varphi}_l} \tilde{\mathbf{\Lambda}}^{(l)} - \mathbf{I} \right) \tilde{\mathbf{H}} \mathbf{B}^T \tilde{\mathbf{x}}_u + e^{-j\hat{\varphi}_l} \mathbf{v} \\ &= e^{-j\hat{\varphi}_l} \tilde{\mathbf{\Lambda}}^{(l)} \tilde{\mathbf{H}} \mathbf{G}_d \mathbf{d}^{(l)} + \mathbf{e}^{(l)} + e^{-j\hat{\varphi}_l} \mathbf{v}, \end{aligned} \quad (10)$$

with $\mathbf{e}^{(l)}$ denoting the residual UW and pilot offset. Assuming that CPE correction already compensates the CFO effects sufficiently, i.e., $e^{-j\hat{\varphi}_l} \tilde{\mathbf{\Lambda}}^{(l)} \approx \mathbf{I}$, we have $\mathbf{e}^{(l)} \approx \mathbf{0}$ and obtain a simplified linear system model

$$\tilde{\mathbf{y}}^{(l)} \approx \tilde{\mathbf{H}} \mathbf{G}_d \mathbf{d}^{(l)} + e^{-j\hat{\varphi}_l} \mathbf{v}. \quad (11)$$

⁴We neglect the potential leakage of $\tilde{\mathbf{x}}_u$ parts from the zero to the non-zero subcarriers due to ICI.

For this system model and with $\mathbb{E}\{\mathbf{d}^{(l)}\mathbf{d}^{(l)H}\} = \sigma_d^2\mathbf{I}$, a linear minimum mean square error (LMMSE) estimator [41] given as

$$\mathbf{E}_{\text{LMMSE}} = (\mathbf{G}_d^H \tilde{\mathbf{H}}^H \tilde{\mathbf{H}} \mathbf{G}_d + \frac{N\sigma_d^2}{\sigma_v^2} \mathbf{I})^{-1} \mathbf{G}_d^H \tilde{\mathbf{H}}^H \quad (12)$$

is a good choice to estimate the data symbols as

$$\hat{\mathbf{d}}^{(l)} = \mathbf{E}_{\text{LMMSE}} \tilde{\mathbf{y}}^{(l)}. \quad (13)$$

The k th element of $\hat{\mathbf{d}}^{(l)}$ follows as

$$\hat{d}^{(l)}[k] = e^{-j\hat{\varphi}_l} e^{j\varphi_l} \mathbf{e}_k^T \tilde{\mathbf{\Lambda}}_{\text{stat}} \tilde{\mathbf{H}} \mathbf{g}_k d^{(l)}[k] + \Delta_k + e^{-j\hat{\varphi}_l} \mathbf{e}_k^T \mathbf{v}, \quad (14)$$

with $\mathbf{e}_k^T = [\mathbf{E}_{\text{LMMSE}}]_{k,*}$, $\mathbf{g}_k = [\mathbf{G}_d]_{*,k}$, $\tilde{\mathbf{\Lambda}}_{\text{stat}} = \mathbf{B}^T \tilde{\mathbf{\Lambda}}'_{\text{stat}} \mathbf{B}$, $\tilde{\mathbf{\Lambda}}_{\text{stat}} \in \mathbb{C}^{(N-N_z) \times (N-N_z)}$, and

$$\Delta_k = e^{-j\hat{\varphi}_l} e^{j\varphi_l} \mathbf{e}_k^T \tilde{\mathbf{\Lambda}}_{\text{stat}} \tilde{\mathbf{H}} \sum_{m=0, m \neq k}^{N_d-1} \mathbf{g}_m d^{(l)}[m]. \quad (15)$$

The estimate $\hat{d}^{(l)}[k]$ in (14) consists of a corrupted version of $d^{(l)}[k]$, an impairment by the other data symbols Δ_k due to ICI, and an additive noise term. We keep the latter for model completeness to be available for further utilization in subsequent sections. However, in order to reveal the CFO effects, we set $\mathbf{v} = \mathbf{0}$ for the following considerations. Before we conduct MSE analyses on $\hat{\mathbf{d}}^{(l)}$, let us first determine the impact of $\hat{\varphi}_l$ on $\hat{\mathbf{d}}^{(l)}$ by examining two CPE estimator variants.

1) *Perfect CPE estimation*: We start with a perfect CPE estimator given as $\hat{\varphi}_l = \varphi_l$. Next, we introduce a magnitude phase model $a_{d,k} e^{j\varphi_{d,k}} = \mathbf{e}_k^T \tilde{\mathbf{\Lambda}}_{\text{stat}} \tilde{\mathbf{H}} \mathbf{g}_k$ in (14) to represent the impairment on the k th data symbol as

$$\hat{d}_{\text{perf}}^{(l)}[k] = a_{d,k} e^{j\varphi_{d,k}} d^{(l)}[k] + \Delta_k \approx e^{j\varphi_{d,k}} d^{(l)}[k] + \Delta_k. \quad (16)$$

The approximation $a_{d,k} \approx 1$ relies on an estimator cancelling out the impact of the channel and generator matrix such that $\mathbf{e}_k^T \tilde{\mathbf{H}} \mathbf{g}_k \approx 1$, and the approximation $|\tilde{\mathbf{\Lambda}}_{\text{stat}}| \approx \mathbf{I}$ [38].

The estimate $\hat{d}_{\text{perf}}^{(l)}[k]$ in (16) deviates from the transmitted symbols $d^{(l)}[k]$ by $\varphi_{d,k}$ and Δ_k , causing a phase rotation and an expansion of single data points to clouds, respectively. Both, UW-OFDM and CP-OFDM, suffer from Δ_k (although with different power levels), but the existence of $\varphi_{d,k}$ is limited to UW-OFDM only, cf. Fig. 4. It originates from the combination of \mathbf{G}_d distributing a data symbol across neighboring subcarriers and ICI leaking back parts of it, thus resulting in a self-interference of $d^{(l)}[k]$.

2) *Non-perfect pilot tone based CPE estimation*: Following [36], an estimate $\hat{\varphi}_l$ based on the pilot tones \mathbf{p} is given as

$$\hat{\varphi}_l = \varphi_l + \varphi_p + \delta_l, \quad (17)$$

which deviates from φ_l by an additive random deviation δ_l and a phase offset φ_p caused by self interference of the pilot symbols. The latter originates from the same underlying effect as $\varphi_{d,k}$. Incorporating (17) into (14) yields

$$\hat{d}_{\text{non-p}}^{(l)}[k] \approx e^{-j(\varphi_l + \varphi_p + \delta_l)} e^{j\varphi_l} e^{j\varphi_{d,k}} d^{(l)}[k] + \Delta_k \approx e^{j\varphi_{\text{off}}} d^{(l)}[k], \quad (18)$$

with a remaining and approximated offset $\varphi_{\text{off}} = \frac{1}{N_d} \sum_{k=0}^{N_d-1} \varphi_{d,k} - \varphi_p = \varphi_d - \varphi_p$. For this approximation, we

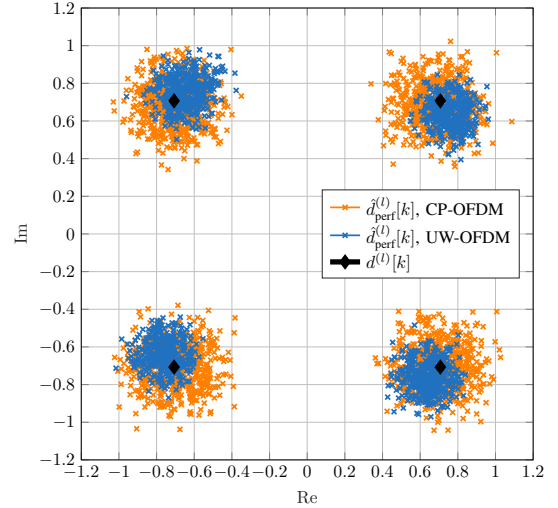


Figure 4: Constellation diagram of $\hat{\mathbf{d}}^{(l)}$ for $\hat{\varphi}_l = \varphi_l$, QPSK, $\tilde{\mathbf{H}} = \mathbf{I}$, $\tilde{\mathbf{x}}_u = \mathbf{0}$, $\mathbf{e}^{(l)} = \mathbf{0}$, $\epsilon = 0.1$, $l = 0, \dots, L-1$, and $\sigma_v^2 = 0$.

neglect the minor impact of δ_l and use an averaged offset φ_{off} with φ_d for all subcarriers, as there is almost no performance difference compared to subcarrier individual offsets with $\varphi_{d,k}$ [38]. We refine the estimate in (13) by incorporating the effect of φ_{off} . Additionally, we refrain from the approximation $e^{-j\hat{\varphi}_l} \tilde{\mathbf{\Lambda}}^{(l)} \approx \mathbf{I}$, which is the underlying basis for the simplified model of $\tilde{\mathbf{y}}^{(l)}$ in (11), yielding now

$$\begin{aligned} \hat{\mathbf{d}}^{(l)} &= e^{-j\hat{\varphi}_{\text{off}}} \mathbf{E}_{\text{LMMSE}} \tilde{\mathbf{y}}^{(l)} \\ &= e^{-j\hat{\varphi}_{\text{off}}} e^{-j\hat{\varphi}_l} \mathbf{E}_{\text{LMMSE}} \tilde{\mathbf{\Lambda}}^{(l)} \tilde{\mathbf{H}} \mathbf{G}_d \mathbf{d}^{(l)} + e^{-j\hat{\varphi}_{\text{off}}} \mathbf{E}_{\text{LMMSE}} \mathbf{e}^{(l)} \\ &\quad + e^{-j\hat{\varphi}_{\text{off}}} e^{-j\hat{\varphi}_l} \mathbf{E}_{\text{LMMSE}} \mathbf{v}. \end{aligned} \quad (19)$$

We obtain an estimate $\hat{\varphi}_{\text{off}}$ according to

$$\hat{\varphi}_{\text{off}} = \hat{\varphi}_d - \hat{\varphi}_p = (m_d - m_p) \hat{\epsilon}, \quad (21)$$

with $m_d, m_p \in \mathbb{R}$ derived from numerical evaluations that depend on the UW-OFDM setup and $\tilde{\mathbf{H}}$, and an estimate $\hat{\epsilon}$ based on (5) with the details in [36].

For the subsequent evaluations, we use the same systems and assume the same multipath channels as propagation environment as for the BER simulations later on, with the setups detailed in Sec. V-A. We utilize a Barker code as \mathbf{x}_u [42] for the non-zero case, and scale the samples to yield equal average power compared to the rest of the symbol. We estimate $\hat{\varphi}_l$ based on pilot tones [36] with the error given in (17), and $\hat{\epsilon}$ once per packet [36] based on (5).

Fig. 5 shows the Bayesian MSE (BMSE) per data symbol $\theta_d = \frac{1}{L} \sum_{l=0}^{L-1} \frac{1}{N_d} \mathbb{E} \left\{ \left\| \hat{\mathbf{d}}^{(l)} - \mathbf{d}^{(l)} \right\|_2^2 \right\}$ as a function of the CFO ϵ . UW-OFDM outperforms CP-OFDM ($\mathbf{G}_{d,\text{cp}}$) for all investigated setups, which is due to the reduced intercarrier/interdata effects compared to CP-OFDM, and follows from a property inherited from the special UW-OFDM generator matrix structures [36].

The overlapping and two most lower curves in Fig. 5 (solid blue line for \mathbf{G}'_d and solid orange line for \mathbf{G}''_d) represent

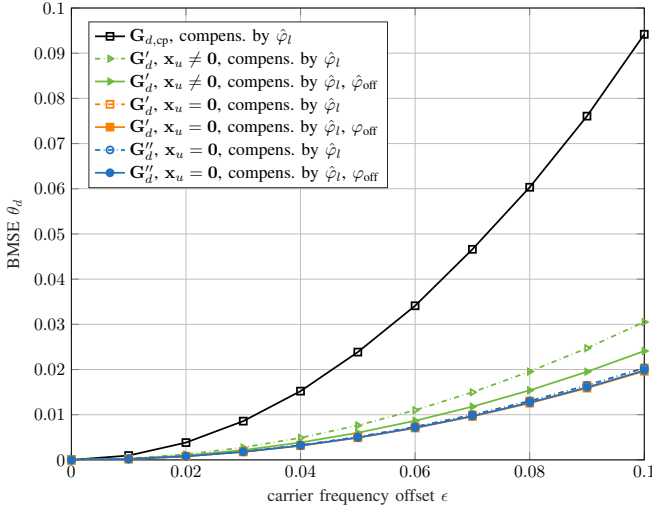


Figure 5: BMSE θ_d of $\hat{\mathbf{d}}^{(l)}$ from (13) and (19) for UW-OFDM and CP-OFDM ($\mathbf{G}_{d,\text{cp}}$) with $l = 0, \dots, L-1$, $\sigma_d^2 = 1$, and $\sigma_v^2 = 0$.

bounds for an optimal performance in this scenario (i.e., zero UW, $\mathbf{e}^{(l)} = \mathbf{0}$ and $\hat{\varphi}_{\text{off}} = \varphi_{\text{off}}$). Comparing with the case without offset compensation as depicted by the (overlapping) dashed lines slightly above, we conclude that the gain of the latter is rather limited in the zero UW case.

Obviously, the performance gain due to phase offset compensation is more dominant in the non-zero UW case. It increases with the CFO value and is almost the same regardless of compensating by φ_{off} or only by an estimate $\hat{\varphi}_{\text{off}}$ (thus only the latter is shown). For the non-zero UW case, results are limited to \mathbf{G}'_d , as the zero UW scenario already confirmed a similar CFO robustness of \mathbf{G}'_d and \mathbf{G}''_d .

The most lower curve in Fig. 5 confirms that even in the best case of CPE correction, there is still room for improvement due to an incomplete CFO cancellation. Closing the remaining performance gap will thus be tackled in the subsequent section.

B. Advanced CFO Compensation Techniques

Next, we aim at decreasing the MSE that remains after applying the methods presented in the preceding section even further, relying on the methods proposed in [38]. With (10), $\mathbf{x}_u = \mathbf{0}$ and with $\mathbf{e}^{(l)} = \mathbf{0}$, the system model can be written as

$$\tilde{\mathbf{y}}^{(l)} = e^{-j\hat{\varphi}_l} \tilde{\mathbf{\Lambda}}^{(l)} \tilde{\mathbf{H}} \mathbf{G}_d \mathbf{d}^{(l)} + e^{-j\hat{\varphi}_l} \mathbf{v}. \quad (22)$$

With an estimate $\hat{\varphi}_l$ according to (17), we obtain

$$\tilde{\mathbf{y}}^{(l)} = e^{-j(\varphi_l + \varphi_p + \delta_l)} \tilde{\mathbf{\Lambda}}^{(l)} \tilde{\mathbf{H}} \mathbf{G}_d \mathbf{d}^{(l)} + e^{-j(\varphi_l + \varphi_p + \delta_l)} \mathbf{v} \quad (23)$$

$$= e^{-j(\varphi_p + \delta_l)} \tilde{\mathbf{\Lambda}}_{\text{stat}} \tilde{\mathbf{H}} \mathbf{G}_d \mathbf{d}^{(l)} + e^{-j(\varphi_l + \varphi_p + \delta_l)} \mathbf{v}. \quad (24)$$

Aside from δ_l (which has only a minor impact [36]), all OFDM symbols experience the same remaining CFO impairments, which can be fully compensated by multiplying with $e^{j\varphi_p} \tilde{\mathbf{\Lambda}}_{\text{stat}}^{-1}$. As φ_p and $\tilde{\mathbf{\Lambda}}_{\text{stat}}$ depend on ϵ , only estimates of them

are available. Applying $e^{j\hat{\varphi}_p} \hat{\mathbf{\Lambda}}_{\text{stat}}^{-1}$ on $\tilde{\mathbf{y}}^{(l)}$ followed by $\mathbf{E}_{\text{LMMSE}}$ from (12), a data estimate is obtained as

$$\hat{\mathbf{d}}^{(l)} = \mathbf{E}_{\text{LMMSE}} e^{j\hat{\varphi}_p} \hat{\mathbf{\Lambda}}_{\text{stat}}^{-1} \tilde{\mathbf{y}}^{(l)} \quad (25)$$

$$= e^{j(\hat{\varphi}_p - \varphi_p - \delta_l)} \mathbf{E}_{\text{LMMSE}} \hat{\mathbf{\Lambda}}_{\text{stat}}^{-1} \tilde{\mathbf{\Lambda}}_{\text{stat}} \tilde{\mathbf{H}} \mathbf{G}_d \mathbf{d}^{(l)} \quad (26)$$

$$+ e^{j(\hat{\varphi}_p - \varphi_p - \delta_l - \varphi_l)} \mathbf{E}_{\text{LMMSE}} \hat{\mathbf{\Lambda}}_{\text{stat}}^{-1} \mathbf{v}.$$

As a matrix inversion denotes an additional, non-negligible computational overhead, we draw on the similarities of $\tilde{\mathbf{\Lambda}}_{\text{stat}}$ with a unitary matrix, cf. (6), and approximate

$$\tilde{\mathbf{\Lambda}}_{\text{stat}}^{-1} \approx \tilde{\mathbf{\Lambda}}_{\text{stat}}^H, \quad (27)$$

yielding

$$\hat{\mathbf{d}}^{(l)} = e^{j(\hat{\varphi}_p - \varphi_p - \delta_l)} \mathbf{E}_{\text{LMMSE}} \hat{\mathbf{\Lambda}}_{\text{stat}}^H \tilde{\mathbf{\Lambda}}_{\text{stat}} \tilde{\mathbf{H}} \mathbf{G}_d \mathbf{d}^{(l)} \quad (28)$$

$$+ e^{j(\hat{\varphi}_p - \varphi_p - \delta_l - \varphi_l)} \mathbf{E}_{\text{LMMSE}} \hat{\mathbf{\Lambda}}_{\text{stat}}^H \mathbf{v}.$$

Fig. 6 confirms for \mathbf{G}'_d a significant gain by applying the proposed advanced CFO compensation methods. Please note that we observed very similar results for \mathbf{G}''_d , but omit them here for the sake of clarity. The remaining gap to the performance bound with perfect conditions, i.e., $\tilde{\mathbf{\Lambda}}_{\text{stat}}^{-1}$, $\hat{\varphi}_l$, and φ_p (note that φ_p compensates for $\hat{\varphi}_l \neq \varphi_l$ up to δ_l), shows only a minor performance degradation due to the applied approximations. Offset compensation becomes more relevant compared to the results in Sec. III-A, as φ_p and φ_d do not cancel each other as it is partially the case in (20). In absolute terms, the gain due to additional offset compensation is approximately doubled when comparing to simple CPE correction by $\hat{\varphi}_l$ (Fig. 5). Also CP-OFDM benefits significantly from the advanced methods and the gap to UW-OFDM is reduced in comparison to Fig. 5. However, UW-OFDM remains the better scheme.

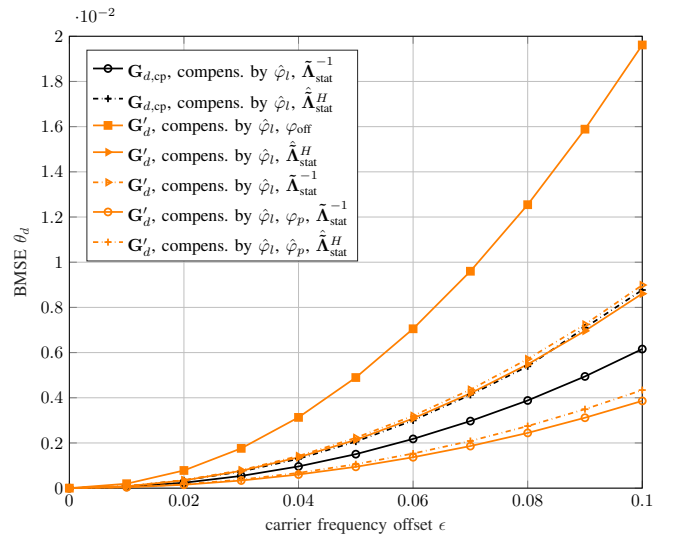


Figure 6: BMSE θ_d of $\hat{\mathbf{d}}^{(l)}$ (28) for advanced CFO compensation methods with $\mathbf{x}_u = \mathbf{0}$, $\mathbf{e}^{(l)} = \mathbf{0}$, $l = 0, \dots, L-1$, $\sigma_d^2 = 1$ and $\sigma_v^2 = 0$.

IV. DERIVATION OF ANALYTICAL ERROR MODEL FOR RESIDUAL CFO IMPAIRMENTS

The compensation methods presented in Sec. III are not capable of perfectly canceling the CFO impairments, but will leave a certain residual error. In this section, we will derive an analytical signaling model describing the residual CFO induced error after data estimation. Once an error model is available, this information can then serve as a basis for deriving reliability information in the form of e.g., bit log-likelihood ratios (LLRs) and fed to a channel decoder in the receiver. We will do so in Sec.V. For the calculation of the bit LLRs, we rely on the derivations in [43], which assume as underlying model

$$\hat{r} = se^{j\theta} + w, \quad (29)$$

with $s \in \mathbb{A}$ denoting a transmitted symbol distorted by a residual phase error given as $\theta \sim \mathcal{N}(0, \sigma_\theta^2)$ and AWGN given as $w \sim \mathcal{CN}(0, 2\sigma_w^2)$. In order to utilize the same LLR calculation scheme, we have to bring the UW-OFDM signaling model into the form of (29). Based on this model, bit LLRs can easily be derived by carrying out the equations in [43], which are left out here for reasons of compactness⁵.

Starting from (14) and compensating for the offset in (18), an estimate of a single data symbol follows as

$$\hat{d}^{(l)}[k] = e^{j(\varphi_l - \hat{\varphi}_l)} e^{-j\hat{\varphi}_{\text{off}}} \mathbf{e}_k^T \tilde{\Lambda}_{\text{stat}} \tilde{\mathbf{H}} \mathbf{g}_k d^{(l)}[k] \quad (30)$$

$$+ e^{-j\hat{\varphi}_{\text{off}}} \Delta_k + e^{-j\hat{\varphi}_{\text{off}}} e^{-j\hat{\varphi}_l} \mathbf{e}_k^T \mathbf{v} \quad (31)$$

$$= \alpha_k d^{(l)}[k] e^{j\theta_l} + w. \quad (32)$$

We note that (32) coincides with (29), whereas $\alpha_k = e^{-j\hat{\varphi}_{\text{off}}} \mathbf{e}_k^T \tilde{\Lambda}_{\text{stat}} \tilde{\mathbf{H}} \mathbf{g}_k$ denotes a complex-valued scaling factor such that $\alpha_k \hat{d}^{(l)}[k] \equiv s$, and $w = e^{-j\hat{\varphi}_{\text{off}}} \Delta_k + e^{-j\hat{\varphi}_{\text{off}}} e^{-j\hat{\varphi}_l} \mathbf{e}_k^T \mathbf{v}$ is modelled as AWGN distributed according to $w \sim \mathcal{CN}(0, \sigma_w^2)$ with

$$\sigma_w^2 = \mathbb{E} \{ \Delta_k \Delta_k^H \} + \mathbb{E} \{ \mathbf{e}_k^T \mathbf{v} \mathbf{v}^H \mathbf{e}_k^* \}. \quad (33)$$

The assumption of a Gaussian distribution for w seems justified, given that $\mathbf{v} \sim \mathcal{CN}(0, \sigma_v^2 \mathbf{I})$, see (7), and considering the law of large numbers in case of Δ_k , see (15). Further, $\theta_l = \varphi_l - \hat{\varphi}_l$ represents the residual phase error with an assumed distribution of $\theta_l \sim \mathcal{N}(0, \sigma_\theta^2)$. In order to verify this assumption, we have to investigate the estimate $\hat{\varphi}_l$ in detail and derive σ_θ^2 accordingly.

Throughout this work, we utilize a CPE estimation approach [36] given as

$$\hat{\varphi}_l = \arg \left(\mathbf{p}^H \mathbf{W}_p \hat{\mathbf{p}}^{(l)} \right), \quad (34)$$

where $\mathbf{W}_p = \text{diag}(\mathbf{w}_p)$, $\mathbf{w}_p \in \mathbb{R}^{N_p \times 1}$, forms a diagonal weighting matrix and $\hat{\mathbf{p}}^{(l)} \in \mathbb{C}^{N_p \times 1}$ incorporates the estimated pilot symbols from the l th OFDM symbol. According to [36], the m th estimated pilot symbol is given as

$$\hat{p}^{(l)}[m] = [\mathbf{E}_p]_{m,*} \tilde{\Lambda}_h^{(l)} (\mathbf{G}_p \mathbf{p} + \mathbf{B}^T \tilde{\mathbf{x}}_u) + v'''[m]$$

⁵We note that this work with $w \sim \mathcal{CN}(0, \sigma_w^2)$ and [43] with $w \sim \mathcal{CN}(0, 2\sigma_w^2)$ use slightly different definitions for a complex Gaussian distribution, which has to be accounted for in the LLR derivations.

$$= \mathbf{e}_m^T e^{j\varphi_l} \tilde{\Lambda}_{h,\text{stat}} (\mathbf{g}_m p[m] + \mathbf{B}^T \tilde{\mathbf{x}}_u) + v'''[m], \quad (35)$$

with $\mathbf{e}_m^T = [\mathbf{E}_p]_{m,*}$, $\mathbf{E}_p \in \mathbb{N}^{N_p \times (N - N_z)}$ denoting a pilot subcarrier selection matrix, $\mathbf{g}_m = [\mathbf{G}_p]_{*,m}$, $\tilde{\Lambda}_{h,\text{stat}} = \tilde{\mathbf{H}}^{-1} \tilde{\Lambda}_{\text{stat}} \tilde{\mathbf{H}}$, and $v'''[m]$ denoting an additive noise term detailed further in the subsequent paragraphs. Inserting (35) into (34) together with introducing the notation

$$a_p e^{j\varphi_p} = \sum_{m=0}^{N_p-1} w_p[m] \mathbf{e}_m^T \tilde{\Lambda}_{h,\text{stat}} (\mathbf{g}_m |p[m]|^2 + \mathbf{B}^T \tilde{\mathbf{x}}_u p[m]^H) \quad (36)$$

yields

$$\hat{\varphi}_l = \arg \left(\mathbf{p}^H \mathbf{W}_p \hat{\mathbf{p}}^{(l)} \right) \quad (37)$$

$$= \arg \left(\sum_{m=0}^{N_p-1} p[m]^H w_p[m] \hat{p}^{(l)}[m] \right) \quad (38)$$

$$= \arg \left(e^{j\varphi_l} e^{j\varphi_p} + \frac{1}{a_p} \sum_{m=0}^{N_p-1} v'''[m] w_p[m] p[m]^H \right) \quad (39)$$

$$= \varphi_l + \varphi_p + \delta_l, \quad (40)$$

whereas δ_l represents an additive deviation approximated by

$$\delta_l \approx f \left(\frac{1}{a_p} \sum_{k=0}^{N_p-1} v'''[m] w_p[m] p[m]^H \right), \quad (41)$$

with some proper function $f(\cdot)$ modelling this approximation. Following [44], it holds that for any $\alpha \in [0, 2\pi[$, $\beta \in \mathbb{R}$, and $n \sim \mathcal{CN}(0, \sigma_n^2)$, an estimate $\hat{\alpha}$ can be well approximated as

$$\hat{\alpha} = \arg(\beta e^{j\alpha} + n) \approx \alpha + n_\alpha \quad (42)$$

with $n_\alpha \sim \mathcal{N}(0, \frac{1}{2}\sigma_n^2)$, given that $|\beta|^2 \gg \sigma_n^2$. Applying the approximation in (42) on (40) and (41) requires further elaboration of $v'''[m]$. As detailed in [36], $v'''[m]$ consists of the three additive terms

$$v'''[m] = p_{\text{ICI}}^{(l)}[m] + d_{\text{ICI}}^{(l)}[m] + v''[m], \quad (43)$$

which denote the m th element of the respective vectors $\mathbf{p}_{\text{ICI}}^{(l)} \in \mathbb{C}^{N_p \times 1}$, $\mathbf{d}_{\text{ICI}}^{(l)} \in \mathbb{C}^{N_p \times 1}$ and $\mathbf{v}'' \in \mathbb{C}^{N_p \times 1}$ defined as

$$\mathbf{p}_{\text{ICI}}^{(l)} = \mathbf{E}_p \tilde{\mathbf{H}}^{-1} \tilde{\Lambda}^{(l)} \tilde{\mathbf{H}} \mathbf{G}_p \mathbf{p} - \mathbf{p}, \quad (44)$$

$$\mathbf{d}_{\text{ICI}}^{(l)} = \mathbf{E}_p \tilde{\mathbf{H}}^{-1} \tilde{\Lambda}^{(l)} \tilde{\mathbf{H}} \mathbf{G}_d \mathbf{d}, \quad (45)$$

$$\mathbf{v}'' = \mathbf{E}_p \tilde{\mathbf{H}}^{-1} \mathbf{B}^T \mathbf{v}. \quad (46)$$

In this case, $\mathbf{p}_{\text{ICI}}^{(l)}$ denotes a constant offset due to ICI induced by the other pilot symbols, $\mathbf{d}_{\text{ICI}}^{(l)}$ a data induced ICI and \mathbf{v}'' AWGN. With a mean μ due to the pilot subcarrier induced ICI given as $\mu = \frac{1}{a_p} \sum_{m=0}^{N_p-1} w_p[m] p[m]^H p_{\text{ICI}}^{(l)}[m]$, under the assumption of $\mathbb{E} \{ d_{\text{ICI}}^{(l)}[m] v''[m]^H \} = 0$ and with $\sigma_{d_{\text{ICI}},m}^2 = \mathbb{E} \{ d_{\text{ICI}}^{(l)}[m] d_{\text{ICI}}^{(l)*}[m]^H \}$ and $\sigma_{v''_m}^2 = \mathbb{E} \{ v''[m] v''[m]^H \}$, we obtain

$$\sigma_{n_\alpha}^2 = \frac{1}{2} \mathbb{E} \left\{ (n - \mu) (n - \mu)^H \right\} \quad (47)$$

$$\equiv \sigma_\theta^2 \quad (48)$$

$$= \frac{1}{2|a_p|^2} \sum_{m=0}^{N_p-1} |w_p[m]|^2 |p[m]|^2 \left(\sigma_{d_{\text{ICI},m}}^2 + \sigma_{v_m''}^2 \right). \quad (49)$$

The Gaussian distribution assumption of (49) is justified based on the same arguments as for w , cf. (33). We note that (42) assumes $\mu = \mathbb{E}\{n\} = 0$. Although this is not entirely fulfilled for the UW-OFDM signaling model due to $p_{\text{ICI}}^{(l)}[m]$, we further note that pilot symbols are usually approximately uniformly distributed over the entire subcarrier set to optimize estimation performance of system parameters [45]. Consequently, the pilot symbols are several subcarriers apart from each other, resulting in a rather minor ICI due to $\mathbf{p}_{\text{ICI}}^{(l)}$, which therefore justifies an assumption of $\mu \approx 0$.

As a last step, we still have to incorporate the constant phase offset φ_p within $\hat{\varphi}_l$ from (40) into our model by introducing

$$\alpha'_k = \alpha_k e^{j\varphi_p}, \quad (50)$$

thus yielding the final signal model

$$\hat{d}^{(l)}[k] = \alpha'_k d^{(l)}[k] e^{-j\theta_l} + w, \quad (51)$$

whereas $\theta \sim \mathcal{N}(0, \sigma_\theta^2)$ with σ_θ^2 given in (49) as well as $w \sim \mathcal{CN}(0, \sigma_w^2)$ with σ_w^2 defined in (33). We note that for the advanced compensation methods tackling ICI impairments as well, see Sec. III-B, we assume $\mathbb{E}\{\Delta_k \Delta_k^H\} \stackrel{!}{=} 0$ within σ_w^2 . Based on this model, bit LLRs can easily be derived following the equations in [43], which concludes the derivations for the underlying signaling model.

V. BIT ERROR RATIO SIMULATIONS

In the following, we will present BER simulations for coded as well as uncoded transmission in a frequency selective environment. So far, CFO effects have been considered in this work in isolation to separate its influence on UW-OFDM from other degrading effects. As such, we intentionally relied on the simplifying assumption of $\sigma_v^2 = 0$. In this section, we investigate the CFO impairments w.r.t. a full UW-OFDM communication system and thus consider $\sigma_v^2 \neq 0$. We note that this work substantially extends the BER analysis conducted in previous works, as up till now BER assessments have either been restricted to considerations without CFO impairments [2], or the receiver did not incorporate accurate information on the residual CFO impairments in the decoding process [38].

A. Simulation setup

We generate UW-OFDM packets with $L = 200$ UW-OFDM symbols and process them as depicted in Fig. 7. We apply a rate $r = 1/2$ convolutional code with constraint length 7 and generator polynomial $(133; 171)_8$ as channel encoder, as well as a code of rate $r = 3/4$ derived from the $r = 1/2$ code according to the puncturing pattern $\begin{pmatrix} 1 & 1 & 0 \\ 1 & 0 & 1 \end{pmatrix}$. The encoded bits are interleaved within one UW-OFDM packet. We note that the interleaver length is different compared to an interleaver restricted to one OFDM symbol as utilized in some of our previous works [1], [2], [6], [38], [7], which therefore may impede a direct comparison of the BER results in some cases. However, a change of the interleaver length is necessary to prevent statistical dependencies among the bits

Table I: Main parameters of the utilized UW-OFDM and CP-OFDM setup.

		UW-OFDM	CP-OFDM
DFT size	N	64	64
data subcarriers	N_d, N'_d	32	48
zero subcarriers	N_z	12	12
pilot subcarriers	N_p	4	4
red. subcarriers	N_r	16	-
guard interval samples	N_g, N_u	16	16
zero subcarrier indices	\mathcal{I}_z	{0,27,28,...,37}	{0,27,28,...,37}
pilot subcarrier indices	\mathcal{I}_p	{7,21,43,57}	{7,21,43,57}
DFT length	T_{DFT}	3.2 μs	3.2 μs
guard interval length	T_{GI}	0.8 μs	0.8 μs
OFDM symbol length	T_{OFDM}	3.2 μs	4 μs
subcarrier spacing	Δ_f	312.5 kHz	312.5 kHz

within an OFDM symbol l , which are otherwise present due to a common error introduced by the estimate $\hat{\varphi}_l$, resulting then in a degradation of the decoding performance at the receiver. QPSK and QAM16 serve as modulation alphabet and \mathbf{G}'_d as well as \mathbf{G}''_d are applied as generator matrices. Soft decision Viterbi decoding is applied at the receiver, with the reliability information provided in form of LLRs derived from the signaling models for $\hat{d}^{(l)}$ given in (20) and (28) for simple CPE and advanced CFO compensation, respectively, and with the detailed model derivations presented in Sec. IV.

We scale the utilized UW-OFDM generator matrices \mathbf{G}'_d and \mathbf{G}''_d such that $\mathbf{G}'_d{}^H \mathbf{G}'_d = \alpha \mathbf{I}$ and $\mathbf{G}''_d{}^H \mathbf{G}''_d = \alpha \mathbf{I}$ with $\alpha = N'_d/N_d$, whereas N'_d corresponds to the number of CP-OFDM data subcarriers. This scaling will provide a fair comparison with CP-OFDM, as it ensures for both the same data induced mean power per non-pilot subcarrier, which directly effects the level of data induced ICI disturbances, see (15). In fact, it is even slightly in favor of CP-OFDM, as the spreading by $\mathbf{G}_p \mathbf{p}$ adds up to the total mean power per non-pilot subcarrier. We use $\mathbf{G}_{d,\text{cp}} = \mathbf{B}_p \mathbf{I}$ and $\mathbf{G}_{p,\text{cp}} = \mathbf{P}_p [\mathbf{I} \quad \mathbf{0}^T]^T$ to model CP-OFDM. Furthermore, Tab. I presents the relevant setup parameters of the investigated UW-OFDM and CP-OFDM systems.

BER results are obtained by averaging over 10^4 independent channel realizations, with the channel impulse responses normalized to unit energy and following an exponentially decaying power delay profile [46] with a given channel delay spread of $\tau_{\text{RMS}} = 100$ ns. We have carried out simulations for several CFO values in the range $0 \leq \epsilon \leq 0.1$, but we only show results for 0 and 0.1 to enhance clarity in the figures. All other results fall within the corridor spanned by those boarder values. Additionally, BER results for the case without CFO serve as principle performance bounds in the following figures. Since the pilot subcarriers are utilized for estimating φ_l , we choose $\mathbf{x}_u = \mathbf{0}$. Except for the bounds, all results presented in Figs. 8–13 always incorporate a CFO compensation by multiplying the l th OFDM symbol with $e^{-j(\hat{\varphi}_l + \hat{\varphi}_{\text{off}})}$, which is thus omitted in the legend.

The estimate $\hat{\varphi}_l$ in (17) follows from $\hat{\varphi}_l = \arg(\mathbf{p}^H \mathbf{W}_p \hat{\mathbf{p}}^{(l)})$ with $\mathbf{W}_p = |\hat{\mathbf{H}}_p|^2$ and $\hat{\mathbf{H}}_p \in \mathbb{C}^{N_p \times N_p}$ denoting a diagonal matrix with the channel frequency response coefficients cor-

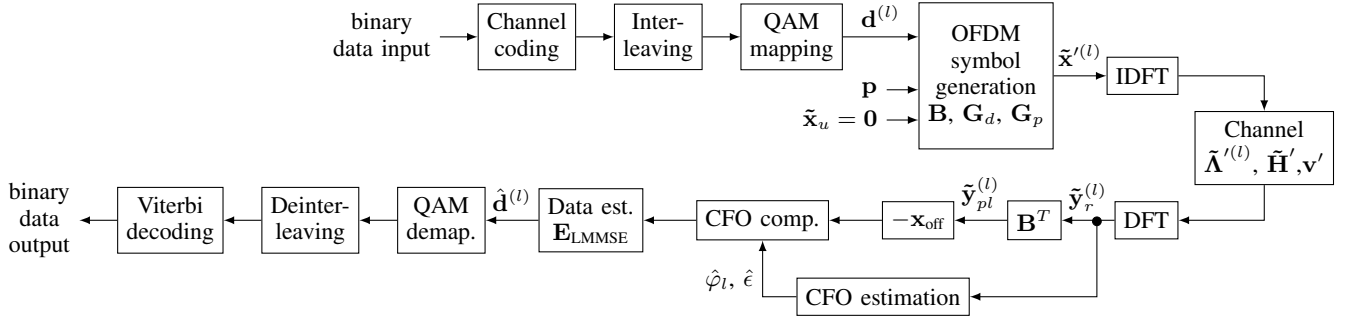


Figure 7: Block diagram of the considered UW-OFDM transceiver system.

responding to the pilot subcarriers on its main diagonal. For all systems we apply a simple pilot subcarrier extraction matrix $\mathbf{E}_p = [\mathbf{0} \ \mathbf{I}] \mathbf{P}_p^T$ to estimate $\hat{\mathbf{p}}^{(l)}$. The phase offset $\hat{\varphi}_{\text{off}}$ is estimated based on the model stated in (21), with the details given in [36]. We assume perfect knowledge of the channel and evaluate performance differences among systems at a BER of 10^{-6} .

B. Results

The MSE analyses conducted in Sec. III-A showed a very similar robustness of \mathbf{G}'_d and \mathbf{G}''_d against CFO and thus an almost identical performance in terms of this error metric. However, the same findings cannot not be expected per se for BER considerations of a complete communication transceiver chain. As laid out in e.g., [2], UW-OFDM systems with different generator matrices show a quite different BER behavior depending on the transceiver chain, e.g., the properties of the wireless channel or the coding rate of the applied channel code. As such, individual investigations of \mathbf{G}'_d and \mathbf{G}''_d are necessary in the following. In Fig. 8, we compare UW-OFDM (\mathbf{G}'_d and \mathbf{G}''_d) against CP-OFDM ($\mathbf{G}_{d,\text{cp}}$) for $\epsilon = 0$ and $\epsilon = 0.1$ in case of uncoded transmission. Both UW-OFDM systems significantly outperform CP-OFDM in the high E_b/N_0 regime, with superior performance of \mathbf{G}'_d . While all three systems experience a saturating BER behavior for $\epsilon = 0.1$ eventually, this happens for \mathbf{G}'_d not before the very low BER regime. For all systems, considerations without CFO slightly deviate from $\epsilon = 0$, but this is only noticeable in lower E_b/N_0 regimes (see zoom in Fig. 9). The reason for this difference is due to the CFO estimation algorithm incorrectly detecting $\hat{\epsilon} \neq 0$ (due to $\hat{\varphi}_l \neq 0$) instead of $\epsilon = 0$, leading to a performance gap to curves without CFO, with the latter representing the performance bound of $\epsilon = 0$ and error free detection. Fig. 10 shows BER results for coded transmission for $r = 1/2$. UW-OFDM with \mathbf{G}'_d outperforms CP-OFDM in all three considered scenarios, namely by 1.6 dB in case without CFO, 0.3 dB for $\epsilon = 0$ and 1.0 dB for $\epsilon = 0.1$. Analyzing the system performances individually, we note that UW-OFDM shows a 1 dB larger performance loss than CP-OFDM when moving from the idealized scenario without CFO to $\epsilon = 0$. However, UW-OFDM is significantly less sensitive to an increase of ϵ , as can be seen when comparing the cases for $\epsilon = 0$ and $\epsilon = 0.1$. In line with [2] showing also results without CFO but for a slightly different system setup (i.e., no pilot subcarriers), UW-

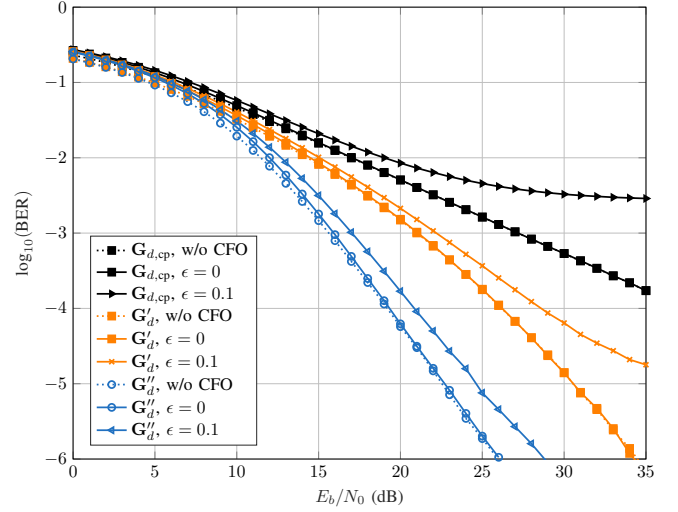


Figure 8: BER results for uncoded transmission and QPSK.

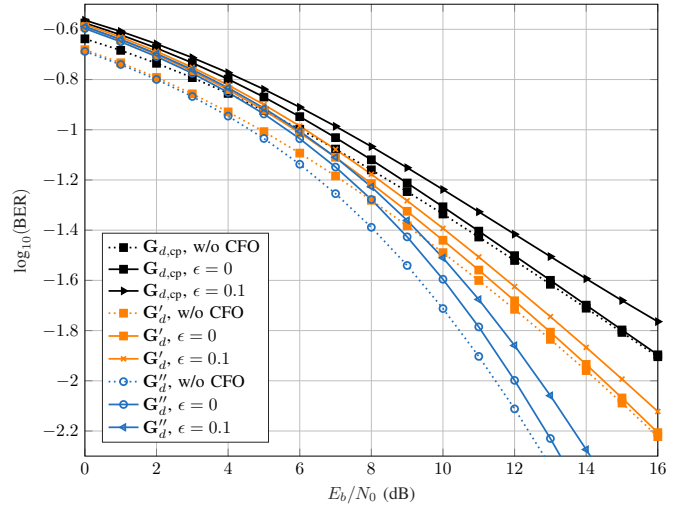


Figure 9: BER results for uncoded transmission and QPSK (zoom of Fig. 8).

OFDM with \mathbf{G}''_d and CP-OFDM perform very similar for a low coding rate. While the same still holds true for $\epsilon = 0$, \mathbf{G}''_d offers the same gain of 1.0 dB over CP-OFDM for $\epsilon = 0.1$ as \mathbf{G}'_d . For $r = 3/4$, the advantages of UW-OFDM due to CFO robustness (both, \mathbf{G}'_d and \mathbf{G}''_d) even increase compared

to $r = 1/2$, see Fig. 11. As for $r = 1/2$, scenarios without CFO outperform $\epsilon = 0$, but the difference is less prominent and reduces with increasing E_b/N_0 , as the impact of the estimation error in $\hat{\varphi}_l$ on the BER performance becomes less relevant. Figs. 12 and 13 show the BER performance for

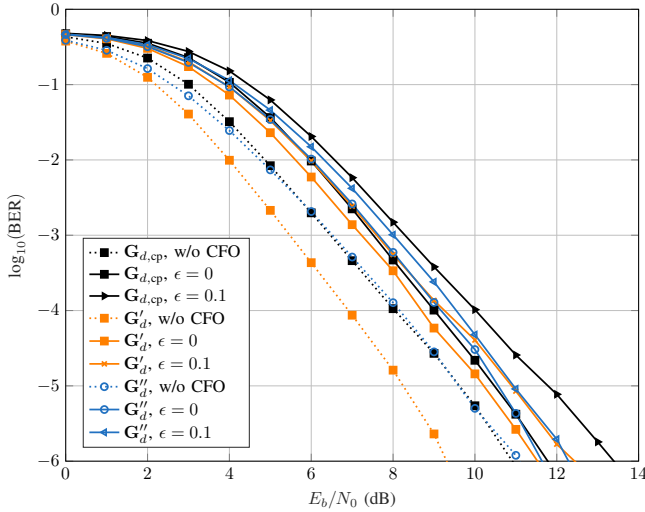


Figure 10: BER results for coded transmission with $r = 1/2$ and QPSK.

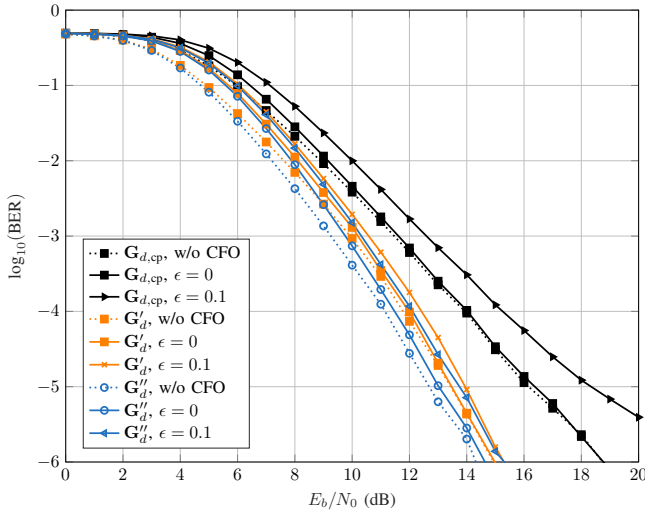


Figure 11: BER results for coded transmission with $r = 3/4$ and QPSK.

$r = 1/2$ and $r = 3/4$, respectively, when utilizing QAM16 as a representative for higher-order modulation alphabets. While in the low CFO case (i.e., w/o CFO and $\epsilon = 0$), only \mathbf{G}'_d may outperform CP-OFDM, the superiority of UW-OFDM becomes independent of the specific generator matrix instance and for an increasing CFO, as illustrated by the case $\epsilon = 0.1$ and the thereof resulting saturating BER behavior of CP-OFDM.

In a next step, we will extend BER performance considerations from simple CPE correction by $\hat{\varphi}_l$ (see Sec. III-A) to the advanced methods presented in Sec. III-B. We limit ourselves to results for \mathbf{G}'_d only to enhance clarity in the figures, knowing though that these sophisticated methods provided

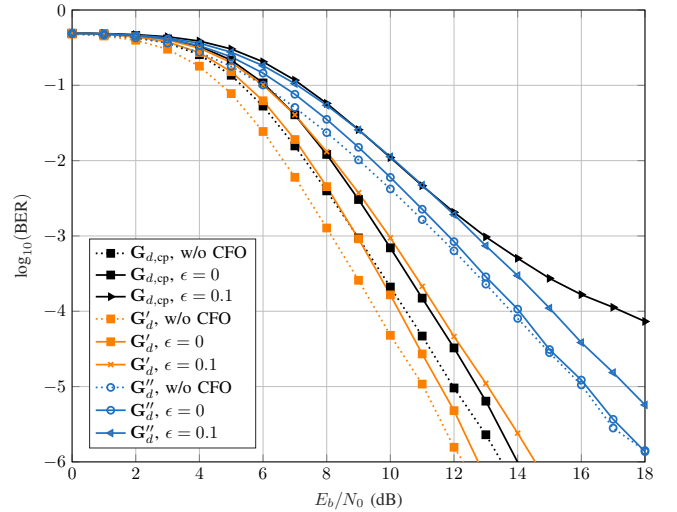


Figure 12: BER results for coded transmission with $r = 1/2$ and QAM16.

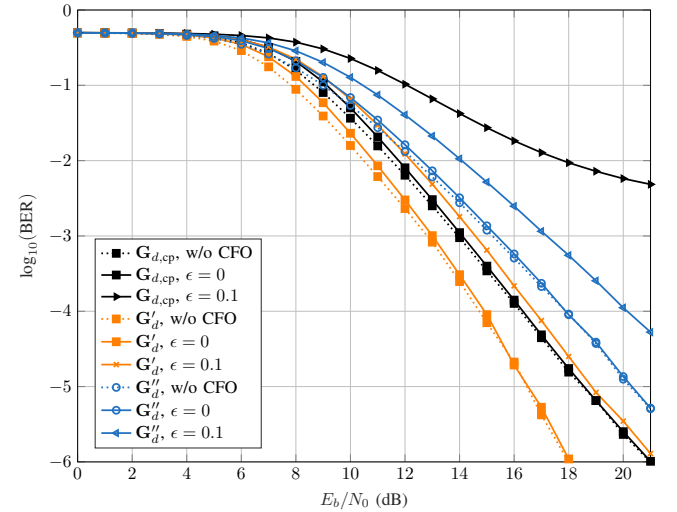


Figure 13: BER results for coded transmission with $r = 3/4$ and QAM16.

the same qualitative performance gain when we conducted the same experiments with \mathbf{G}''_d . Since a considerable gain on top of CPE correction is only applicable for the high CFO regime, see Fig. 6, investigations are limited to $\epsilon = 0.1$. Furthermore, our BER simulations demonstrated an increasing gain with an increasing order of the modulation alphabet, we thus restrict elaborations to QAM16. Two advanced methods are considered on top of CPE correction by $\hat{\varphi}_l$, namely φ_p in combination with $\tilde{\Lambda}_{\text{stat}}^{-1}$ serving as a principle performance bound, as well as $\hat{\varphi}_p$ together with $\hat{\Lambda}_{\text{stat}}^H$ denoting a low complexity implementation thereof, where we obtain $\hat{\epsilon}$ from averaging over 200 single estimates of 200 OFDM symbols. Fig. 14 depicts for UW-OFDM and CP-OFDM in each case four curves, with two serving as reference. These two reference curves have already been part of Fig. 12 and show the performance for simple CPE correction in case of $\epsilon = 0$ and $\epsilon = 0.1$ for a coded transmission with $r = 1/2$. We

note that for UW-OFDM the complexity reduced version with $\hat{\varphi}_p$ and $\hat{\tilde{\Lambda}}_{\text{stat}}^H$ coincides with the performance bound given by compensating with φ_p and $\tilde{\Lambda}_{\text{stat}}^{-1}$. These two methods improve simple CPE compensation by another 1.4 dB and thus reduce the margin to the case of $\epsilon = 0$ to 0.5 dB. Improvements are also obtained for CP-OFDM, however, the saturating BER behavior can unfortunately not fully be canceled. The benefit of advanced CFO compensation methods even increases for $r = 3/4$. Fig. 15 reveals for UW-OFDM a 2.2 dB gain over CPE compensation, leaving a residual gap of 0.5 dB to the performance in case of $\epsilon = 0$. For CP-OFDM, we observe the same behavior as for $r = 1/2$, with the advanced compensation methods again only partially combating a saturating BER performance. As already stated, please note that for G_d'' we obtained the same conclusions as for G_d' , i.e., a significant reduction of the residual gap between $\epsilon = 0$ and $\epsilon = 0.1$, and only a minor performance loss due to approximations in the compensation method.

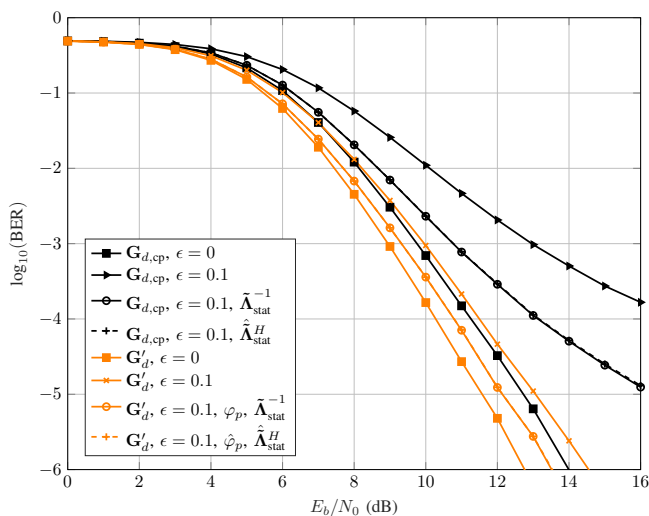


Figure 14: BER results for coded transmission with $r = 1/2$ and QAM16.

We conclude that the methods presented in this section provide a valuable performance gain over CPE correction at only moderate additional computational complexity. Since inverting unitary matrices simplifies to taking the complex conjugate of the matrix elements, the additional overhead of the methods presented is essentially limited to a single matrix-vector multiplication per UW-OFDM symbol.

VI. CONCLUSION

In this work we have shown that UW-OFDM offers a better CFO robustness than CP-OFDM based on MSE analyses. Moreover, the performance gap increases along an increasing CFO. Various CFO compensation approaches have been considered, from simple CPE correction to advanced CFO compensation, and the remaining errors have been derived analytically. Furthermore, a system level based assessment in terms of the BER performance of a whole transceiver chain has been conducted. Uncoded as well as coded transmission

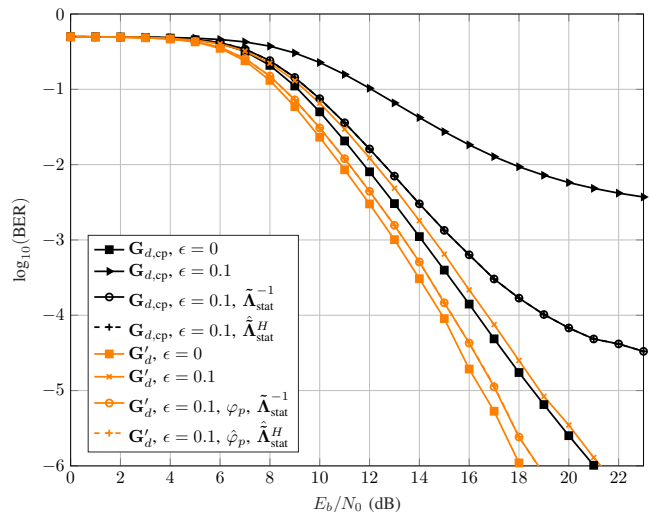


Figure 15: BER results for coded transmission with $r = 3/4$ and QAM16.

in a frequency selective environment confirmed the superiority of UW-OFDM over CP-OFDM with respect to CFO impairments.

REFERENCES

- [1] M. Huemer, C. Hofbauer, and J. B. Huber, "The Potential of Unique Words in OFDM," in *Proc. 15th Int. OFDM Workshop*, Hamburg, Sep. 2010, pp. 140–144.
- [2] M. Huemer, C. Hofbauer, and J. Huber, "Non-Systematic Complex Number RS Coded OFDM by Unique Word Prefix," *IEEE Trans. Signal Process.*, vol. 60, no. 1, pp. 285–299, Jan. 2012.
- [3] M. Rajabzadeh, H. Steendam, and H. Khoshbin, "Power Spectrum Characterization of Systematic Coded UW-OFDM Systems," in *Proc. IEEE Veh. Technol. Conf. (VTC Fall)*, Las Vegas, NV, USA, Sep. 2013, p. 5.
- [4] M. Rajabzadeh, H. Khoshbin, and H. Steendam, "Sidelobe Suppression for Non-Systematic Coded UW-OFDM in Cognitive Radio Networks," in *Proc. Europ. Wireless Conf.*, Barcelona, Spain, May 2014, pp. 826–831.
- [5] M. Rajabzadeh and H. Steendam, "Power Spectral Analysis of UW-OFDM Systems," *IEEE Trans. Commun.*, vol. 66, no. 6, pp. 2685–2695, Jun. 2018.
- [6] M. Huemer, A. Onic, and C. Hofbauer, "Classical and Bayesian Linear Data Estimators for Unique Word OFDM," *IEEE Trans. Signal Process.*, vol. 59, no. 12, pp. 6073–6085, Dec. 2011.
- [7] C. Hofbauer, C. Böck, and M. Huemer, "From Dedicated Redundant Subcarriers to Distributed Redundancy in UW-OFDM," in *Proc. Asilomar Conf. Signals, Systems and Computers*, Nov. 2016, pp. 1099–1103.
- [8] Z. A. H. Qasem, J. Wang, X. Kuai, H. Sun, and H. Esmail, "Enabling Unique Word OFDM for Underwater Acoustic Communication," *IEEE Wireless Commun. Lett.*, vol. 10, no. 9, pp. 1886–1889, 2021.
- [9] S. A. Cheema, J. Zhang, M. Huemer, and M. Haardt, "Linear detection schemes for MIMO UW-OFDM," in *Proc. Asilomar Conf. Signals, Systems and Computers*, 2016, pp. 1457–1461.
- [10] M. Huemer, C. Hofbauer, A. Onic, and J. B. Huber, "On the Exploitation of the Redundant Energy in UW-OFDM: LMMSE Versus Sphere Detection," *IEEE Signal Process. Lett.*, vol. 19, no. 6, pp. 340–343, Jun. 2012.
- [11] A. Onic and M. Huemer, "Noise Interpolation for Unique Word OFDM," *IEEE Signal Process. Lett.*, vol. 21, no. 7, pp. 814–818, Jul. 2014.
- [12] A. Onic, "Receiver Concepts for Unique Word OFDM," Ph.D. dissertation, Institute of Networked and Embedded Systems, Alpen-Adria-Universität Klagenfurt, Nov. 2013.
- [13] H. Steendam, "Theoretical Performance Evaluation and Optimization of UW-OFDM," *IEEE Trans. Commun.*, vol. 64, no. 4, pp. 1739–1750, Apr. 2016.

- [14] C. Douillard, M. Jezequel, C. Berrou, A. Picar, P. Didier, and A. Glavieux, "Iterative Correction of Intersymbol Interference: Turbo Equalization," *Proc. Eur. Trans. Telecommun. (ETT)*, vol. 6, no. 3, pp. 507–511, Sep. 2012.
- [15] M. Tuechler, A. C. Singer, and R. Koetter, "Minimum Mean Squared Error Equalization using a Priori Information," *IEEE Trans. Signal Process.*, vol. 50, no. 3, pp. 673–683, Mar. 2002.
- [16] W. Haselmayr, C. Hofbauer, B. Etlzinger, A. Springer, and M. Huemer, "Iterative Detection for Unique Word OFDM," in *Proc. Conf. Global Commun. (Globecom)*, Austin, TX, USA, Dec. 2014, pp. 3261–3266.
- [17] W. Haselmayr, C. Hofbauer, M. Huemer, and A. Springer, "Approaching the Matched Filter Bound with Unique Word OFDM," in *Proc. IEEE Int. Conf. Commun. (ICC)*, May 2019, pp. 1–4.
- [18] S. Baumgartner, G. Bognár, O. Lang, and M. Huemer, "Neural Network Approaches for Data Estimation in Unique Word OFDM Systems," *IEEE Trans. Veh. Technol.*, pp. 1–16, 2023.
- [19] G. Bognár, S. Baumgartner, O. Lang, and M. Huemer, "Neural Network Optimal UW-OFDM," in *Proc. Asilomar Conf. Signals, Systems and Computers*, 2021, pp. 389–394.
- [20] M. Muck, M. de Courville, and P. Duhamel, "A Pseudorandom Postfix OFDM Modulator—Semi-Blind Channel Estimation and Equalization," *IEEE Trans. Signal Process.*, vol. 54, no. 3, pp. 1005–1017, Mar. 2006.
- [21] D. V. Welden, H. Steendam, and M. Moeneclaey, "Iterative DA/DD Channel Estimation for KSP-OFDM," in *Proc. IEEE Int. Conf. Commun. (ICC)*, Beijing, China, May 2008, pp. 693–697.
- [22] S. Tang, F. Yang, K. Peng, C. Pan, K. Gong, and Z. Yang, "Iterative Channel Estimation for Block Transmission with Known Symbol Padding — A New Look at TDS-OFDM," in *Proc. Conf. Global Commun. (Globecom)*, Washington, DC, USA, Nov. 2007, pp. 4269–4273.
- [23] "Framing Structure, Channel Coding and Modulation for Digital Television Terrestrial Broadcasting System," Chinese National Standard, Std. GB 20 600-2006, 2006.
- [24] C. yen Ong, J. Song, C. Pan, and Y. Li, "Technology and Standards of Digital Television Terrestrial Multimedia Broadcasting [Topics in Wireless Communications]," *IEEE Commun. Mag.*, vol. 48, no. 5, pp. 119–127, May 2010.
- [25] L. Jingyi, W. Hai, P. Joo, and J. Ro, "The Effect of Filling Unique Words to Guard Interval for OFDM System," C802.16a-02/87, IEEE 802.16 Broadband Wireless Access Working Group, Sep. 2002.
- [26] M. Rajabzadeh and H. Steendam, "Precoding for PAPR Reduction in UW-OFDM," *IEEE Commun. Lett.*, vol. 25, no. 7, pp. 2305–2308, 2021.
- [27] J. B. Huber, J. Rettelbach, M. Seidl, and M. Huemer, "Signal Shaping for Unique-Word OFDM by Selected Mapping," in *Proc. Europ. Wireless Conf.*, Poznan, Poland, Apr. 2012, p. 8.
- [28] J. Rettelbach and J. B. Huber, "PMR-Reduction for Continuous Time OFDM Transmit Signals by Selected Mapping," in *Proc. Int. Symp. Signals, Syst. and Electron. (ISSE)*, Potsdam, Germany, Oct. 2012.
- [29] A. Onic and M. Huemer, "Limiting the Complexity of Sphere Decoding for UW-OFDM," in *Proc. Int. OFDM Workshop*, Hamburg, Sep. 2011, pp. 135–139.
- [30] "IEEE Std 802.11a-1999, Part 11: Wireless LAN Medium Access Control (MAC) and Physical Layer (PHY) specifications: High-Speed Physical Layer in the 5 GHz Band," IEEE, 1999.
- [31] L. Deneire, B. Gyselinckx, and M. Engels, "Training Sequence versus Cyclic Prefix—A New Look on Single Carrier Communication," *IEEE Commun. Lett.*, vol. 5, no. 7, pp. 292–294, Jul. 2001.
- [32] H. Witschnig, T. Mayer, M. Petit, H. Hutzelmann, A. Springer, and R. Weigel, "The Advantages of a Unique Word for Synchronisation and Channel Estimation in a SC/FDE System," in *Proc. Europ. Mobile Comm. Conf.*, Apr. 2003, pp. 436–440.
- [33] A. Aboltins, "Carrier Frequency Offset Estimator based on Unique Word Cross-Correlation," in *Proc. Telecomm. Forum (TELFOR)*, Nov. 2012, pp. 486–489.
- [34] K. Kim and H. Park, "Enhanced Phase Tracking for Unique Word based SC-FDE on Frequency Selective Channels," in *Proc. Int. Microw. Workshop Series RF Front-ends Softw. Def. and Cogn. Radio Sol. (IMWS)*, Apr. 2010, p. 4.
- [35] S. Ehsanfar, M. Chaffi, and G. Fettweis, "A Study on Unique-Word based Synchronization for MIMO Systems over Time-Varying Channels," in *Proc. Wireless Comm. Netw. Conf. (WCNC)*, Seoul, Korea, Apr. 2020, pp. 1–7.
- [36] C. Hofbauer, W. Haselmayr, H.-P. Bernhard, and M. Huemer, "On the Inclusion and Utilization of Pilot Tones in Unique Word OFDM," *IEEE Trans. Signal Process.*, vol. 68, pp. 5504–5518, 2020.
- [37] C. Hofbauer, W. Haselmayr, and M. Huemer, "Pilot Tone Insertion and Utilization in Unique Word OFDM," in *Proc. Int. Workshop Signal Proc. Adv. Wireless Comm. (SPAWC)*, Atlanta, GA, USA, May 2020, p. 5.
- [38] C. Hofbauer, "Design and Analysis of Unique Word OFDM," Ph.D. dissertation, Institute of Networked and Embedded Systems, Alpen-Adria-Universität Klagenfurt, Jun. 2016.
- [39] C. Hofbauer, W. Haselmayr, H.-P. Bernhard, and M. Huemer, "Impact of a Carrier Frequency Offset on Unique Word OFDM," in *Proc. Int. Symp. Pers., Indoor and Mobile Radio Comm. (PIMRC)*, London, UK, Sep. 2020, p. 7.
- [40] M. Huemer, C. Hofbauer, A. Onic, and J. B. Huber, "Design and Analysis of UW-OFDM Signals," *Int. J. Electron. and Commun. AEU*, vol. 68, no. 10, pp. 958–968, Oct. 2014.
- [41] S. M. Kay, *Fundamentals of Statistical Signal Processing, Volume I: Estimation Theory*, 1st ed. Prentice Hall, Apr. 1993.
- [42] S. W. Golomb and R. A. Scholtz, "Generalized Barker Sequences," *IEEE Trans. Inf. Theory*, vol. 11, no. 4, pp. 533–537, Oct. 1965.
- [43] P. Neshaaastegaran and A. H. Banihashemi, "Log-Likelihood Ratio Calculation for Pilot Symbol Assisted Coded Modulation Schemes With Residual Phase Noise," *IEEE Trans. Commun.*, vol. 67, no. 5, pp. 3782–3790, 2019.
- [44] N. Kamiya and E. Sasaki, "Pilot-Symbol Assisted and Code-Aided Phase Error Estimation for High-Order QAM Transmission," *IEEE Trans. Commun.*, vol. 61, no. 10, pp. 4369–4380, 2013.
- [45] X. Cai and G. B. Giannakis, "Error Probability Minimizing Pilots for OFDM with M-PSK Modulation over Rayleigh-Fading Channels," *IEEE Trans. Veh. Technol.*, vol. 53, no. 1, pp. 146–155, Jan. 2004.
- [46] J. Fakatselis, *Criteria for 2.4 GHz PHY Comparison of Modulation*, IEEE Document, 1997, p802.11-97/157r1.